Current Trends in Biotechnology and Pharmacy
Vol. 19(2) 2348-2361, April 2025, ISSN 0973-8916 (Print), 2230-7303 (Online)
DOI: 10.5530/ctbp.2025.2.21

Hydroxyapatite Doped with *Alpinia galanga* (L.) Willd. Rhizome Extract Exhibits Potential Antioxidant and Antibacterial Features

Seethalakshmi Subramaniam[1], Anusuya Nagaraj [1], Suja Samiappan[1,*]

[1] Department of Biochemistry, Bharathiar University, Coimbatore – 641 046, Tamil Nadu

***Corresponding Author**: suja.s@buc.edu.in

Abstract

The study focused on doping of hydroxyapatite (HAp) with *Alpinia galanga* (L.) Willd. rhizome extract (Agr) to impart antioxidant and antimicrobial features to HAp by a green approach. The HAp was synthesized by sol-gel method using ortho-phosphoric acid and calcium nitrate tetrahydrate as precursors. The HAp was doped with Agr by the wet-precipitation method. The X-ray diffraction (XRD) showed that HAp and HAp-Agr biocomposite were crystalline. The FTIR study validated the successful impartation of Agr into HAp by confirming the presence of functional groups as alcoholic, phosphate, and carbonate groups in HAp-Agr biocomposite. The field emission scanning electron microscope analysis showed that HAp and HAp-Agr biocomposite were irregular and agglomerated. Moreover, energy dispersive X-ray (EDX) analysis showed the entrapment of phytomolecules of Agr into HAp-Agr biocomposite. The Zeta potential analysis revealed that HAp and HAp-Agr biocomposite were stable with −24.6 and -10.7 mV, respectively. The hydrodynamic size distribution of HAp and HAp-Agr biocomposite were 191.5 and 280.7 d. nm, respectively. The HAp-Agr biocomposite exhibited potential antioxidant activity, and its IC_{50} value (concentration required to scavenge 50% of free radicals) was 133.92 ± 4.08 and 141.24 ± 6.79 µg/mL in DPPH and ABTS assays, respectively. The HAp-Agr biocomposite exhibited a broad range of antibacterial activity against Gram-ve and Gram+ve bacteria by broth-dilution technique. This work highlighted that the as-synthesized HAp-Agr biocomposite had notable antioxidant and antibacterial characteristics and highly apt for biomedical application.

Keywords: Hydroxyapatite, *Alpinia galanga* (L.) Willd., antioxidant, antibacterial.

Introduction

The swift advancement of modern nanotechnology is broad and utilized in scientific fields, encompassing medical, health, environment, nanoelectronics, national security, etc. Nanotechnology enables the formulation and use of biological, physical, and chemical properties at the molecular or atomic level, particularly within nanoscale dimensions. The rapid progression of nanotechnology in medicine utilizes nanomaterials to monitor, treat, manage, diagnose, and prevent cellular damage induced by infections. Nanomedicine encompasses several biomedical applications, such as dental implants, wound healing, drug delivery, tissue engineering, and medical equipment. The principal aim of nanomedicine is to deliver therapy to the human body at atomic and molecular scales while safeguarding the integrity of healthy cells and tissues (1, 2, 3).

The chemical formula for hydroxyapatite (HAp) is $Ca_{10}(PO_4)_6(OH)_2$, presenting a calcium-to-phosphorus ratio of 1.67. HAp features a hexagonal crystalline structure. The purest form of the powder is white; nevertheless, naturally occurring varieties exhibit brown, yellow, or green types. Nano-hydroxyapatite is the most stable calcium phosphate compound across diverse temperatures, pH levels, and fluid compositions. HAp exhibits biocompatibility, osteoconductivity, bioactivity, non-toxicity, and a non-inflammatory nature. HAp is predominantly utilized in bone and dental enamel applications. HAp can be produced using various techniques, including dry, wet, high-temperature, combination, and biogenic synthesis. These synthesis methods may employ either chemical or naturally occurring precursors. HAp is synthesized from chemical compounds or derived from natural sources, such as animals, marine organisms, shells, plants, and algae. Synthesized HAp using chemical techniques exhibited a substantial surface area, increased porosity, and reduced crystallinity. Surface modification of HAp enhances its characteristics and optimizes its applications. Chemically produced HAp exhibits limited stability and durability, hence constraining its use in the biomedical field. The constraints of synthetically generated HAp prompted the utilization of natural precursors and biopolymers for its manufacture. HAp elicits no adverse reactions in humans, as it is a naturally occurring compound in the body. HAp has several applications, including bone tissue engineering, antimicrobial uses, anticancer therapies, dental implants, bioimaging, and water purification. In bone tissue engineering, HAp is utilized to synthesize new bone tissue and repair bone. The use of HAp in cancer treatment can eradicate neoplastic cells. The doped HAp compositions showed enhanced efficacy in eliminating cancer cells. The production of HAp from chemical or natural sources, including mammalian bones, shells, minerals, and metal ion-doped variants (such as iron, zinc, copper, silver, gold, cerium, and magnesium), demonstrates an inhibitory effect against bacteria (4, 5).

The HAp in dental enamel serves to prevent and reverse cavities, diminish sensitivity, whiten teeth, and ensure non-toxicity and biocompatibility. In several sectors, HAp is extensively utilized in cosmetic applications to enhance skin firmness. It is now used as a hair care product to improve strength and nourish the hair. HAp is used in sunscreen to mitigate UV damage and photoaging. Consequently, HAp is seen as a safer and environmentally beneficial option. Biosynthesized HAp is a potent component with many uses and significant advantages in skeletal, hair, cosmetic, dental, water treatment, and pharmaceutical delivery contexts (6).

Recently, significant attention has been focused on doping HAp with plant extracts. Plants are rich in bioactive substances such as polyphenols, flavonoids, terpenoids, and alkaloids. These substances could exhibit properties such as antibacterial, anti-inflammatory, antioxidant, and potentially osteogenic effects (7, 8). The composite formed by incorporating plant bioactive chemicals into HA may exhibit properties such as antibacterial effects, anti-inflammatory responses, and the promotion of osteoblastogenesis (9, 10).

The present study is focused on the preparation of a composite of HAp with *A. galanga* (L.) Willd. rhizome extract and examine their antioxidant and antibacterial properties. The *Zingiberaceae* family, encompasses *A. galanga* (L.) Willd., also commonly known as galangal or greater galangal, is classified as a perennial plant. This spice is prominently utilized in Indonesian and other Southeast Asian cuisines. This plant is highly significant and is widely employed in traditional medicine in several countries, especially within India's Ayurvedic medicinal system. In Asia, these rhizomes have historically been employed as spices and flavoring agents because of their strong, fragrant fragrances and piquant flavor. A renowned traditional Chinese medication, they have been widely utilized to address gastrointestinal ailments such as indigestion,

gastro-cold vomiting, and abdominal pain. *A. galanga* (L.) Willd. rhizome extract rich with pharmacologically active compounds like β-turmerone, α-turmerone, and cymene (11).

In this study, HAp was prepared by sol-gel method and followed by incorporated with *A. galanga* (L.) Willd. rhizome extract by wet-precipitation method. The HAp and HAp-*A. galanga* (L.) Willd. rhizome extract (HAp-Agr) biocomposite was characterized by nanotechnology approaches. Following, the antioxidant and antibacterial potential of the HAp-Agr biocomposite was demonstrated.

Materials and Methods

Chemicals and reagents

Muller-Hinton agar (MHA), tetracycline, DPPH, ethanol, ABTS, ortho-phosphoric acid (O-PA), ammonia, potassium persulfate, Muller-Hinton broth (MHB), ascorbic acid, methanol, tryptic soy broth, saline, nutrient broth, sodium hydroxide, and calcium nitrate tetrahydrate (CNT) were received from HiMedia, Mumbai, India. The other chemicals and reagents in the study were analytical grade and obtained from Merck, Bengaluru, India. The plasticware was obtained from Tarsons Products, Kolkata, India.

Collection and preparation of plant extract

The fresh rhizomes of *A. galanga* (L.) Willd. were collected from the agriculture market in Coimbatore, India. The rhizomes of *A. galanga* (L.) Willd. were dried for three weeks at room temperature under dark. The dried rhizomes of *A. galanga* (L.) Willd. were ground into powder using the blender. Fifty grams of fine powder were immersed in 250 mL of hydroethanolic at ambient temperature and agitated in a shaker for three days, adopting the cold maceration technique (12). Following this, the hydroethanolic solution was filtered through the Whatman no. 1 filter paper, and the filter was collected. Then, the obtained filtrate was lyophilized at -39°C and concentrated the filtrate. The collected *A. galanga* (L.) Willd. rhizome extract (Agr) was stored at 4°C for further analysis.

Synthesis of HAp and HAp-Agr biocomposite

The *HAp* was prepared using the sol-gel technique (10). The precursor compounds for calcium and phosphate are calcium nitrate tetrahydrate and orthophosphoric acid, respectively. Double distilled water was utilised to make 1 M calcium nitrate tetrahydrate and 0.6 M orthophosphoric acid, each agitated separately for 30 minutes. The orthophosphoric acid solution was added dropwise to the calcium nitrate tetrahydrate solution. The precipitated solution was agitated vigorously for one hour following its introduction. A pH of 10 was maintained, and the solution was kept for 24 hours aging. The precipitate was dried below 200°C in the oven for 6 hours. The obtained product was subjected to furnace treatment for 3 hours at temperatures varying from 300°C to 900°C.

The hydroxyapatite and rhizomes of *A. galanga* (L.) Willd. rhizome extract (HAp-Agr) biocomposite was prepared by the wet-precipitation process (10). In the first step, the equal ratio of HAp and Agr was stirred overnight at 80 rpm in 50 mL of ethanol solution, which confirms an equal mixing of the materials. After that, the precipitated solution was obtained and dried for 24 hours at 35°C in an oven. Finally, the dried sample was ground into a fine powder and sieved.

Characterization of HAp and HAp-Agr biocomposite

To comprehend the crystallinity and phase analysis of the prepared materials, electron-based X-ray diffractometry (XRD) was typically employed. The prepared materials (HAp and HAp-Agr biocomposite) were scanned in the 2theta ranges from 10° to 80° using steps of 0.06° and 10 s of counting time utilizing the diffractometry analysis. The data were then recorded using a Bruker Eco D8 XRD diffractometer (Berlin, Germany) that used Cu-Kα radiation and operated at 40 kV and 25 mA.

The peak locations and intensities are compared with the support of JCPDS (09-432) reference patterns to figure out particle crystallinity (9, 10).

Fourier transform infrared (FTIR) spectroscopy (Shimadzu, Tokyo, Japan) was used to identify the capping and reducing agents as well as the available functional groups in the produced HAp, Agr, and HAp-Agr biocomposite. To acquire the spectrum spanning the 400–4000 cm^{-1} wavelength range, the prepared samples were compressed for two minutes onto a 2-mm disk after being mixed 1:100 with potassium bromide (9, 10).

A field emission scanning electron microscopy (FESEM) with the model name of FEI Quanta 250 FEG-SEM (Thermo Fisher Scientific, USA) was used to investigate the particles' (HAp and HAp-Agr biocomposite) morphological shape and size with the maximum accelerating and operating voltage of 30 kV. The samples were coated with gold sputter coating before image capture. The samples' chemical composition was also recorded in energy dispersive X-rays (EDX) analysis combined with the same microscopy (9, 10).

Similar surface electric charges cause electrostatic repulsion, which makes the dispersion more stable, where the particles are less prone to agglomerate. A measurement of the electric charge at the particle's surface, called zeta potential, is frequently used to evaluate its stability. To determine the average zeta potentials, the prepared samples (HAp and HAp-Agr biocomposite) were dispersed and taken to the Zetasizer with a 60-second analysis period. Further, the samples' hydrodynamic diameter range and polydispersity index (PdI) were measured using dynamic light scattering (DLS) at 25°C with a scattering angle of 90° (Malvern Instruments Ltd, Malvern, United Kingdom) (9, 10).

Antioxidant activity of HAp-Agr biocomposite

DPPH assay

As-synthesized HAp-Agr biocomposite was collected at different concentrations (up to 300 µg/mL), and the volume was standardised to 100 µL using methanol. Approximately 3 mL of a 0.1 mM methanolic solution of DPPH was introduced to the aliquots of HAp-Agr biocomposite and thoroughly vortexed. Ascorbic acid was utilized as the standard. A negative control was established by incorporating 100 µL of methanol into 1 mL of a 0.1 mM methanolic DPPH solution. The tubes were let to remain in the dark for 15 minutes at ambient temperature. The sample's absorbance was measured at 517 nm relative to the blank. The radical scavenging activity of the samples was quantified as IC_{50}, representing the concentration necessary to block 50% of DPPH free radicals concentration (Gunti (13).

ABTS assay

The overall antioxidant activity of the HAp-Agr biocomposite was assessed using the ABTS radical cation decolorisation test. $ABTS^{\bullet+}$ was generated by incubating a 7 mM aqueous solution of ABTS with 2.4 mM potassium persulfate in the dark for 12 to 16 hours at ambient temperature. Before the experiment, this solution was diluted in ethanol (about 1:89, v/v) and equilibrated at 30°C, resulting in an absorbance of 0.700 ± 0.02 at 734 nm. Following the addition of 1 mL of diluted $ABTS^{\bullet+}$ solution to 100 µL of different concentrations of HAp-Agr biocomposite (up to 300 µg/mL). Following, test samples were thoroughly vortexed and incubated in darkness for 30 minutes at room temperature. The standard was ascorbic acid. The absorbance was recorded against the blank at 734 nm (14).

Antibacterial activity of HAp-Agr biocomposite

Minimum inhibitory concentration (MIC)

The antibacterial activity of HAp-Agr biocomposite was tested against Gram-ve bacteria (*Pseudomonas aeruginosa* – MTCC 741, *Escherichia coli* – MTCC 1302, and *Salmonella typhimurium* – MTCC 1254) and Gram+ve bacteria (*Staphylococcus aureus* –

MTCC 740, *Streptococcus pyogenes* – MTCC 0442, and *Bacillus subtilis* – MTCC 1133). To determine the antibacterial effectiveness of HAp-Agr biocomposite, the standard broth dilution method (CLSI M07-A8) was utilized, and it supports the assessment of the visible growth of microbes in the broth (15). Briefly, after the various pure Gram-positive and Gram-negative bacterial cultures had grown overnight distinctly in nutrient broth. The growth density was adjusted to the 1×10^8 CFU/mL concentration using the 0.5 McFarland standard.

First, the microplate wells were filled with 100 µL of Muller Hinton broth (MHB), and then the same volume with different concentrations of HAp-Agr biocomposite (up to 600 µg/mL) was added. Negative control wells without HAp-Agr biocomposite. The positive control is tetracycline. Next, all the wells aside from the negative control well were filled with distinctly 5 µL of bacterial cultures. At OD_{600}, the initial and final spectrum values were obtained before and after incubation (24 hrs). The Synergy H1 plate reader (BioTek, USA) was used to record bacterial growth. The MIC value was predicted by the lowest concentration of HAp-Agr biocomposite, at which no bacterial growth was noticeably present (16).

Minimum bactericidal concentration (MBC)

The Muller Hinton agar (MHA) plates were utilized to assess the MBC of HAp-Agr biocomposite. About 50 µL aliquots were collected from the MIC value (no evident bacterial growth) wells and placed on MH agar plates. They were then incubated for 24 hours at 37°C. Based on visual inspection, the MBC endpoint was identified by the HAp-Agr biocomposite concentration that minimized or killed the bacterial population at ≥ 99.9%. The pre- and post-incubated MHA plates were used to make this observation on the presence or absence of bacteria (17).

Statistical analysis

Three separate runs of the experiment were conducted for antioxidant and antibacterial studies, and the mean ± standard deviation was used to represent the results. One-way ANOVA was used to process the data, and $p < 0.05$ was considered significant.

Results and Discussion

Synthesis and characterization of HAp and HAp-Agr biocomposite

The sol-gel method was used in this study to successfully synthesize HAp using CNT and PA as precursors. After thoroughly washing the synthesized HAp with distilled water to remove NH_4 and NO_3, it was successfully calcined at 900°C. Following this, HAp was doped with Agr using the wet-precipitation method. The resulting combination was dried at 35°C and used for characterization.

XRD analysis

Powder X-ray diffraction (XRD) is a reliable method for determining the compounds' natural phase. With the support of XRD analysis, the sol-gel synthesized HAp and precipitated HAp-Agr biocomposite intense diffractogram patterns as a function of 2θ value are shown in Figure 1. Also, Table 1 presents the respected *hkl* plane numbers of HAp and HAp-Agr biocomposite.

The HAp patterns are initially characterized by distinct and emphasized peaks. The acquired diffracted reflection planes are subjected to HAp, and their hexagonal structure both were proved following the International Centre for Diffraction Data (ICDD) card number [09-0432]. HAp displays a narrow, high, or intense peak, indicating a high degree of crystallinity, and it was found in the distinctive peak at 2theta of 31.28 °C. The study by Niziołek et al. likewise showed a similar pattern of results (18).

In HAp-Agr biocomposite, the recorded characteristic peaks were narrow and intense, and they were recognized to have a similar 2theta range to HAp. Additionally, there were no extra

peaks, and the results from both samples (HAp and HAp-Agr biocomposite) showed that only the crystalline phase was present. However, there was a slight shifting in the diffraction patterns with reduced intensity (low crystalline); it might be due to the phytometabolites' occupation within the HAp pattern, which does not affect its stability (9). Similarly, the green biosynthesized hydroxyapatite-silver nanocomposite mediated by aqueous Indian curry leaf (*Murraya koengii*) extract was characterized by Bee et al. (19). They observed the changes in the slight degree of silver substitution in the apatite lattice during the bio-reduction process that lowers the crystallinity of HAp. Additionally, they showed that the destabilization of HAp was unaffected by the absence of any new peak calcium phosphate phase in the XRD pattern of nanocomposite samples produced by the curry leaf-mediated bio-reduction method.

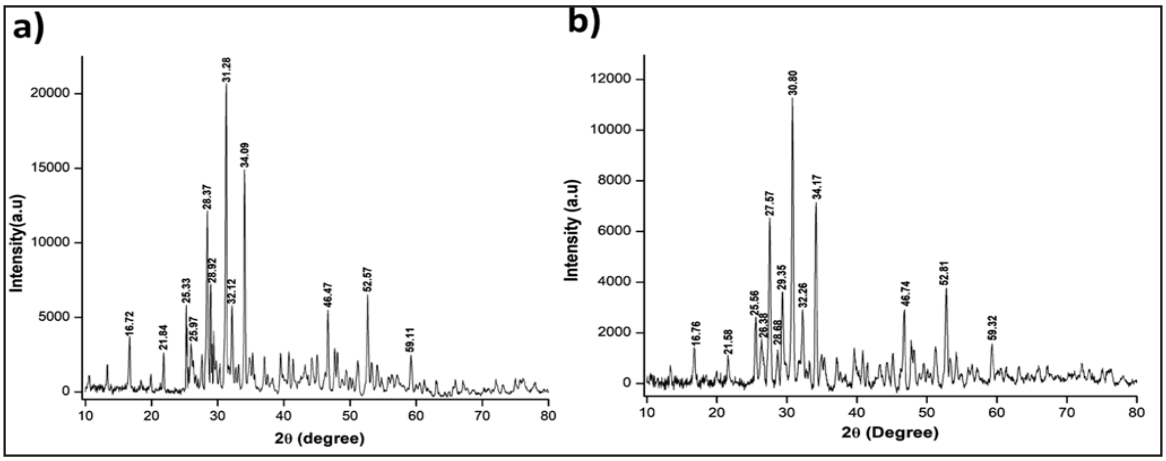

Figure 1: XRD pattern of (a) HAp and (b) HAp-Agr biocomposite.

Table 1: X-ray diffractometric 2theta angle with *hkl* plane numbers for HAp and HAp-Agr biocomposite.

hkl plane number	2theta angle	
	HAp	HAp-Agr biocomposite
101	16.72	16.76
200	21.84	21.58
201	25.33	25.56
002	25.97	26.38
102	28.37	26.68
210	28.92	29.35
211	31.28	30.8
112	32.12	32.26
202	34.09	34.17
222	46.47	46.47
402	52.57	52.81
420	59.11	59.32

FTIR analysis

The characteristic group of frequencies found in a sample provides insight into the nature and purity of the substance. FTIR analysis is an effective and ideal analytical technique used to determine the functional groups and chemical structures of inorganic and organic phases.

According to Figure 2a, the distinctive peaks of HAp are responsible for all of the peaks observed in the FTIR spectra. The peaks are indicative of the symmetric stretching of the O-H group in HAp and can be caused by the presence of absorbed moisture. They appear in the wavenumbers 3438.56, 2922.85 cm^{-1}, and 2084.71 cm^{-1}. The symmetric stretch 1643.59 cm^{-1} may result from carbon dioxide absorption from the atmosphere. Furthermore, PO_4 groups were detected in the synthetic HAp at the distinctive peak 1038.05 cm^{-1} (stretching

of P–O bond), which is very much alike to those seen in naturally occurring hydroxyapatite. The O-P-O group's asymmetric bending modes were shown by the absorption spectral band in the 584.89 cm^{-1} wavenumber. The majority of the PO_4^{3-} group was located in the 400–600 cm^{-1} range of overlapping spectral bands. Thus, it was verified that the manufactured material is HAp based on this functional group observation; additionally, it was remarkably comparable to the results of the previously published studies (20, 21).

The active functional groups from a *Zingiberaceae* family of *A. galanga* (L.) Willd. Rhizome extract's (Agr) phytometabolites were determined using FTIR spectroscopy and are displayed in Figure 2b. The characteristic stretching spectrum length beyond 3000 cm^{-1} is responsible for free hydroxyl groups, which are characteristics of phenolic compounds. The sharp asymmetric absorption band at 2979.07 cm^{-1} indicates the presence of triterpenoids and saponin compounds with C–H stretching of the aliphatic functional group. While the spectral peak at 2895.32 cm^{-1} showed asymmetric and symmetric stretches of alkenes. The vibrational C≡N stretching was found in the 2590.63 cm^{-1} spectral length of the nitrile group of compounds. Absorption at 2333.81 and 1674.99 cm^{-1} represents the vibrational stretching of the C=C group in the aromatic compounds, and at 1404.60 cm^{-1} shows the vibrational bending S=O (sulphate ester) group. The carbonyl group of compounds was found to form a C-O bond at a wavenumber of 1134.22 cm^{-1}. The fingerprint regions of 939.60 cm^{-1} (O-H), 808 cm^{-1} (=CH), and overlapping peaks (579.09 and 503.31 cm^{-1}) of the C=C group of compounds were identified as carboxylic, aromatic, and alkynes, respectively. The ether functional group was visible in the strong absorption bending spectra at 1036.91 cm^{-1}. It was significantly supported by comparing the active functional groups of Agr using the study results of Imchen et al. and Ahmad et al. (22, 23).

In the case of HAp-Agr biocomposite (Fig. 2c), the stretching and bending modes of absorption peaks were identified at 3718.46, 3426.75, 2970.04, 2692.41, 2347.53, 1696.08, 1520.90, 1030.56, and 646.57 cm^{-1}. Also, the IR spectra were obtained using the combined group of HAp and Agr compounds with decreased intensity. Additionally, a shift in the HAp-Agr biocomposite absorption peaks was found, which may be the result of a structural change brought by the functional groups of Agr's active secondary metabolite on the HAp surface. The Agr may also serve as a reducing, stabilizing, and capping agent during the formation of HAp-Agr biocomposite. These encouraging results made it abundantly evident that HAp and Agr had a positive interaction during the composite synthesis process. The findings were highly comparable to those of the Wei et al. study (24). Another work by Das and colleagues reported that, in comparison to synthetic HAp alone, the IR spectrum of simple green synthesized HAp nanoparticles showed altered absorption peaks, indicating a significant interaction between HAp and polydomaine (20).

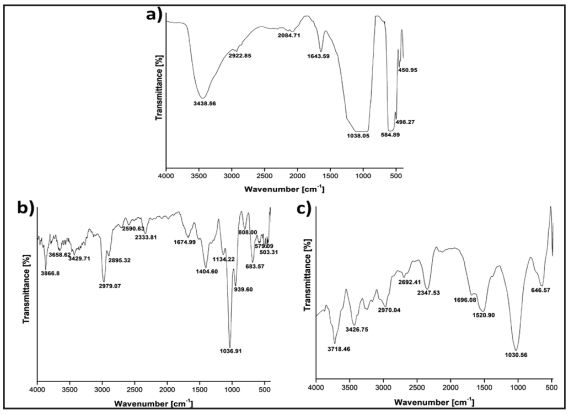

Figure 2: FTIR spectra of (a) HAp, (b), Agr, and (c) HAp-Agr biocomposite.

FESEM analysis

The HAp and HAp-Agr biocomposite morphological shapes are shown in Figure 3. The majority of the HAp particles exhibited irregular faceted shapes with joined boundaries of one crystal to another crystal, according to

the results. The distribution and shape of HAp particles in the composite were made with Agr through the action of adsorption. Still, this covering (adsorption) property of Agr did not affect the morphologies of the HAp particles. Rather, the HAp-Agr biocomposite exhibited an agglomerated cluster-like morphological structure, indicating that only the particles' aggregation and distribution into the HAp are altered.

In addition to morphological observation, Image J software was used to analyze the homogeneity and uniformity of particle dispersion in the studied samples. By counting several approximation particles (50-70), the average size distribution of the manufactured materials was determined to be 227.21 nm (HAp) and 397.99 nm (HAp-Agr biocomposite), respectively, as shown by the histogram (Fig. 4). Because of the particles' propensity to aggregate, the average size of HAp-Agr biocomposite is larger than that of HAp. A similar finding was made by Namasivayam et al., which shows that the average size of free hydroxyapatite nanoparticles is less than that of the triphala-loaded hydroxyapatite nanocomposite, and they postulated that this could be because of the appearance of floccular aggregated particles (25).

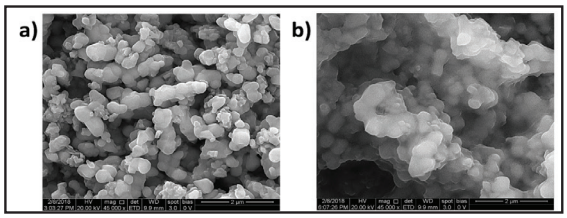

Figure 3: SEM image of (a) HAp and (b) HAp-Agr biocomposite.

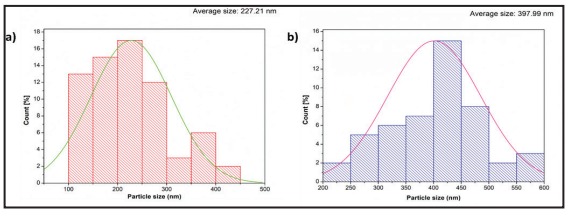

Figure 4: SEM size distribution of (a) HAp and (b) HAp-Agr biocomposite.

EDX analysis

The atomic weight and chemical makeup of virgin HAp, Agr, and HAp-Agr biocomposite were ascertained via energy-dispersive spectrum analyses (Fig. 5 and Table 2). The primary presence of calcium, phosphorous, and oxygen in HAp is shown in Figure 5a. The EDX spectral graph of Agr showed with carbon and oxygen peaks are depicted in Figure 5b. Moreover, the available concentration of carbon in the HAp-Agr biocomposite, together with calcium, phosphorous, and oxygen, was seen in Figure 5c. Thus, as can be seen from the graph, the blended phytomolecules of Agr have been encapsulated with HAp. As a result, FESEM and EDS spectra suggest that HAp and Agr are co-deposited in HAp-Agr biocomposite. According to a study by Vinayagam et al. the HAp formation was shown in the EDX results, where the peaks for calcium, phosphorous, and oxygen were visible. The elemental composition also showed the presence of carbon, which is likely due to the phytochemicals used in the synthesis of *Muntingia calabura*-hydroxyapatite nanoparticles (26).

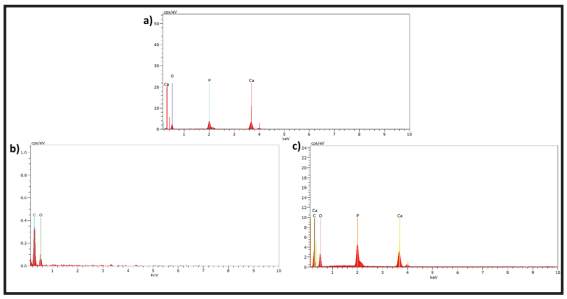

Figure 5: EDX spectra of (a) HAp, (b) Agr, and (c) HAp-Agr biocomposite.

Table 2: Chemical composition of HAp, Agr, and HAp-Agr biocomposite by EXD analysis

Elements	HAp	Agr	HAp-Agr biocomposite
Ca (%)	38.01	—	11.91
P (%)	13.16	—	10.57
O (%)	47.62	27.14	35.02
C (%)	—	70.95	40.57
Total (%)	98.79	98.09	98.07

Current Trends in Biotechnology and Pharmacy
Vol. 19(2) 2348-2361, April 2025, ISSN 0973-8916 (Print), 2230-7303 (Online)
DOI: 10.5530/ctbp.2025.2.21

Zeta potential analysis

Zeta potential can indicate the potential physical stability of the materials prepared under different conditions. The HAp and HAp-Agr biocomposite surface charge and stability features were investigated by measuring their zeta potential values, which are shown in Figure 6. The zeta potential values for HAp and HAp-Agr biocomposite were found to be −24.6 and -10.7 mV, respectively. This value serves as a crucial parameter in assessing the dispersion status and surface charge of the particles because the particles have their electrostatic repulsion, which denotes they are sufficiently strong to maintain their stability. Comparing a coherent result with the Zeta potential of the produced amorphous calcium phosphate family using *Aloe vera* extract, the measurement was −28.7 mV, which is like our study findings (27).

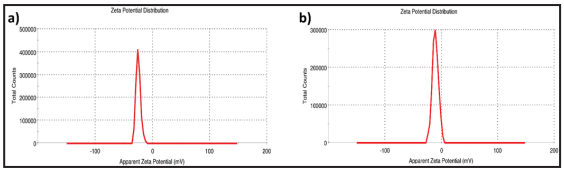

Figure 6: Zeta potential of (a) HAp and (b) HAp-Agr biocomposite.

DLS analysis

The DLS method was used to investigate the particle size distribution of HAp and HAp-Agr biocomposite. The hydrodynamic mean size of HAp and HAp-Agr biocomposite was found to be 191.5 and 280.7 d. nm, respectively (Fig. 7), and this is related to the findings of the FESEM study. Since PDI values below 0.5 are suggestive of monodispersity particles, the polydispersity index (PDI) values of 0.186 (HAp) and 0.719 (HAp-Agr biocomposite) indicated the material's polydisperse nature (28). The supporting study by Abdelmigid and colleagues found that HAp nanoparticles made from *Punica granatum L*. peel, along with the coffee ground extract, had a higher zeta potential negativity of −9.37 mV and -16.9 mV, and the smallest size with 229.6 nm and 167.5 nm, respectively (29). As a result, the produced materials (HAp and HAp-Agr biocomposite) might offer a superior solution in orthopedics. Even Sathiyavimal et al. recently stated that HAp's clinical trial has validated its potential for use as a coating material over orthopedic implants, and research is currently concentrating on HAp in the development of composites for increased strength and efficiency (30).

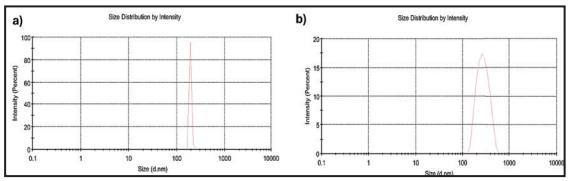

Figure 7: DLS spectra of (a) HAp and (b) HAp-Agr biocomposite

Antioxidant activity of HAp-agr biocomposite

For biomedical applications, improved HAp's capacity to fend off oxidative stress is essential. Osteointegration can be enhanced, and inflammation can be avoided by lowering ROS at the implant-tissue interface. Despite being biocompatible, hydroxyapatite has little intrinsic antioxidant capacity. According to the findings, doping HAp with elements like as cobalt, selenium, silver, zinc, copper, and plant extracts can help overcome these drawbacks by boosting antioxidant activity, enhancing biocompatibility, and possibly supporting medicinal uses (9, 10, 31).

In our study, as-synthesized HAp was doped with *A. galanga* (L.) Willd. rhizome extract by wet-precipitation method and prepared HAp-Agr biocomposite. The antioxidant activity of as-synthesized HAp-Agr biocomposite was assessed by DPPH and ABTS assays. The HAp-Agr biocomposite showed dose-dependent free radical scavenging potential in both DPPH and ABTS free radical scavenging assays (Fig. 8). The IC_{50} value of The HAp-Agr biocomposite was determined as 133.92 ± 4.08 and 141.24 ± 6.79 µg/mL in DPPH and ABTS free radical scavenging assays, respectively.

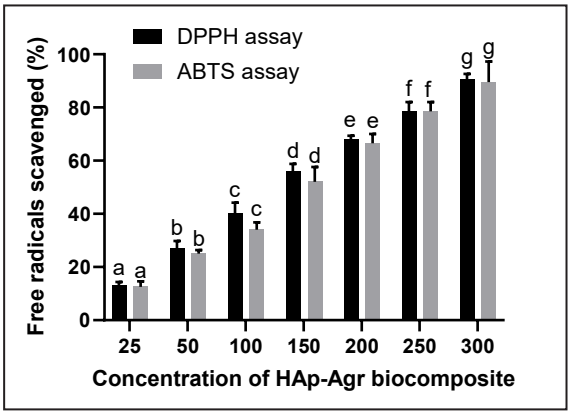

Figure 8: Dose-dependent antioxidant potential of HAp-Agr biocomposite by DPPH and ABTS assay. HAp-Agr biocomposite's dose-dependent antioxidant capability using the DPPH and ABTS assays. Three separate runs of the experiment were conducted, and the mean ± standard deviation was used to represent the results. One-way ANOVA was used to process the data, and $p < 0.05$ was considered significant. The specific study (DPPH or ABTS free radical assay) uses different alphabetical letters to indicate the statistical significance between the various test concentrations of the HAp-Agr biocomposite by Tukey's test.

The HAp doped with metals such as cobalt, copper, zinc, and selenium, as well as plant extracts, introduces redox-active sites that can scavenge free radicals and reduce oxidative stress. This process improves electron transport to counteract free radicals and shield cells from harm caused by ROS (32). The performance of implants and tissue regeneration may be improved by combining the antioxidant HAp with other bioactive substances, such as growth factors. Thus, doping of HAp with plant extracts is quite useful as an oxidative stress reliever in the biomedical field (9, 10, 31).

Antimicrobial activity of HAp-Agr biocomposite

Pure HAp has no antimicrobial activity, which is problematic for implants because bacterial infections (such as biofilm formation) can cause implants to fail. The antimicrobial effectiveness of HAp can be increased by doping it with metal ions and plant extracts (33). However, from the standpoint of biocompatibility, doping HAp with metals is not ideal because it has drawbacks and causes organ toxic effects. Doping HAp with plant extracts, which frequently include natural antimicrobial components, is therefore very ideal and is a recent method to improve its antimicrobial activities while preserving biocompatibility (9, 10).

In our study, as-synthesized HAp-Agr biocomposite through a green chemistry approach has shown potential antimicrobial activity against bacterial pathogens by micro-well dilution technique (Table 3). HAp-Agr biocomposite showed potential antibacterial activity on Gram-ve and Gram+ve bacteria. However, HAp-Agr displayed potentially more significant antimicrobial activity on Gram-ve related to Gram+ve bacteria. Because of their distinct cell wall structure, HAp-Agr biocomposite demonstrated greater antimicrobial action against Gram-negative bacteria. Gram-negative bacteria are particularly vulnerable to damage from HAp-Agr biocomposite because of their thin peptidoglycan layer and lipopolysaccharide outer membrane. The superior antibacterial activity of HAp-Agr biocomposite was observed against Gram-ve bacteria *Pseudomonas aeruginosa* – MTCC 741 with MIC and MBC values of 340.68 ± 12.06 and 428.94 ± 10.71 µg/mL, respectively. The lower antibacterial activity of HAp-Agr biocomposite was observed against Gram+ve bacteria *Bacillus subtilis* – MTCC 1133 with MIC and MBC values of 496.27 ± 18.57 and 620.55 ± 17.24 µg/mL, respectively.

Table 3: The antibacterial potential of HAp-Agr biocomposite by broth-dilution technique.

Bacteria	**MIC (µg/mL)**	**MBC (µg/mL)**
Gram-negative bacteria		
Pseudomonas aeruginosa – MTCC 741	340.68 ± 12.06	428.94 ± 10.71
Escherichia coli – MTCC 1302	372.22 ± 11.84	434.09 ± 14.33
Salmonella typhimurium – MTCC 1254	381.81 ± 12.02	468.26 ± 18.07

Gram-positive bacteria		
Staphylococcus aureus –MTCC 740	470.66 ± 13.68	568.89 ± 21.41
Streptococcus pyogenes – MTCC 0442	483.23 ± 14.71	610.35 ± 18.90
Bacillus subtilis – MTCC 1133	496.27 ± 18.57	620.55 ± 17.24

According to the researchers, bioactive substances such as polyphenols, flavonoids, and terpenoids found in plant extracts have antimicrobial qualities through rupturing bacterial cell membranes, preventing enzyme activity, or obstructing bacterial DNA replication (34, 35, 36). As a result, adding plant extracts to HAp may provide antimicrobial properties. Additionally, doping HAp with plant extracts provides a sustainable and environmentally acceptable substitute for metal doping (9, 10). According to our research, HAp-Agr produced using a green chemistry method is appropriate for orthodontic applications where bacterial infections may cause issues.

Conclusion

The HAp was successfully prepared using the sol-gel approach. The phytomolecules of Agr were imparted into the HAp by wet-precipitation method and fruitfully synthesized HAp-Agr biocomposite. The nanotechnological analysis showed that the as-synthesized HAp-Agr biocomposite was stable, had nano size, crystalline nature, had an irregular shape, and was agglomerated. As-synthesized HAp-Agr biocomposite exhibited potential antioxidant activity under *in-vitro*. Moreover, HAp-Agr biocomposite exhibited a broad range of antibacterial activity against Gram-ve and Gram+ve bacteria. Thus, the study concluded that antioxidant and antibacterial properties were successfully imparted into the HAp from Agr. As-synthesized HAp-Agr biocomposite could be highly applicable as an antioxidant and antimicrobial agent in the orthopaedic field.

Conflict of interest

Authors declare no conflict of interest

Acknowledgements

The authors were thankful to Bharathiar University, Coimbatore, India for providing support and encouragement.

References

1. Salamanca-Buentello, F., and Daar, A. S. (2021). Nanotechnology, equity and global health. *Nature Nanotechnology*, 16(4), 358-361.
2. Rosaiah, G., Mangamuri, U. K., Sikharam, A. S., Devaraj, K., Kalagatur, N. K., Kadirvelu, K., and Vardhan, S. V. M. (2022). Biosynthesis of selenium nanoparticles from *Annona muricata* fruit aqueous extract and investigation of their antioxidant and antimicrobial potentials. *Current Trends in Biotechnology and Pharmacy*, 16(1), 101-107.
3. Lakshmeesha, T. R., Murali, M., Ansari, M. A., Udayashankar, A. C., Alzohairy, M. A., Almatroudi, A., Alomary, M. N., Asiri, S. M. M., Ashwini, B. S., Kalagatur, N. K., Nayak, C. S., and Niranjana, S. R. (2020). Biofabrication of zinc oxide nanoparticles from Melia azedarach and its potential in controlling soybean seed-borne phytopathogenic fungi. *Saudi Journal of Biological Sciences*, 27(8), 1923-1930.
4. Noori, A., Hoseinpour, M., Kolivand, S., Lotfibakhshaiesh, N., Ebrahimi□Barough, S., Ai, J., and Azami, M. (2024). Exploring the various effects of Cu doping in hydroxyapatite nanoparticle. *Scientific Reports*, 14(1), 3421.
5. Liu, Y., Wang, Z., Liu, X., Chen, H., Huang, Y., Li, A., Pu, Y., and Guo, L. (2025). Study on Mechanical Properties, Optical Properties, Cytotoxicity of TiO_2-HAP Nanoparticles-Modified PMMA and Photodynamically Assisted Antibacterial Activity Against *Candida Albicans* in Vitro. *International Journal of Nanomedicine*, 2695-2709.

6. Carella, F., Degli Esposti, L., Adamiano, A., and Iafisco, M. (2021). The use of calcium phosphates in cosmetics, state of the art and future perspectives. *Materials*, 14(21), 6398.
7. Kondabolu, U. L., Babitha, B., Kalagatur, N. K., Nagaraj, A., and Velumani, S. (2023). Phytochemical Analysis in *Pithecellobium dulce* Fruit Peel Extract. *Current Trends in Biotechnology and Pharmacy*, 17(3), 1052-1059.
8. Sathelly, K., Kumar Kalagatur, N., Kiranmayi Mangamuri, U., Obul Reddy Puli, C., and Poda, S. (2022). Anticancer potential of *Solanum lycopersicum* L. extract in human lung epithelial cancer cells A549. *Indian Journal of Biochemistry and Biophysics (IJBB)*, 60(1), 76-85.
9. Nagaraj, A., Kalagatur, N. K., Kadirvelu, K., Shankar, S., Mangamuri, U. K., Sudhakar, P., and Samiappan, S. (2022). Biomimetic of hydroxyapatite with Tridax procumbens leaf extract and investigation of antibiofilm potential in *Staphylococcus aureus* and *Escherichia coli*.
10. Nagaraj, A., and Samiappan, S. (2019). Presentation of antibacterial and therapeutic anti-inflammatory potentials to hydroxyapatite via biomimetic with Azadirachta indica: An in vitro anti-inflammatory assessment in contradiction of LPS-induced stress in RAW 264.7 Cells. *Frontiers in Microbiology*, 10, 1757.
11. Aziz, I. M., Alfuraydi, A. A., Almarfadi, O. M., Aboul-Soud, M. A., Alshememry, A. K., Alsaleh, A. N., and Almajhdi, F. N. (2024). Phytochemical analysis, antioxidant, anticancer, and antibacterial potential of *Alpinia galanga* (L.) rhizome. *Heliyon*, 10(17).
12. George, E., Kasipandi, M., Vekataramana, M., Kumar, K. N., Allen, J. A., Parimelazhagan, T., and Gopalan, N. (2016). In vitro anti-oxidant and cytotoxic analysis of *Pogostemon mollis* Benth. *Bangladesh Journal of Pharmacology*, 11(1), 148-158.
13. Gunti, L., Dass, R. S., and Kalagatur, N. K. (2019). Phytofabrication of selenium nanoparticles from *Emblica officinalis* fruit extract and exploring its biopotential applications: antioxidant, antimicrobial, and biocompatibility. *Frontiers in microbiology*, 10, 931.
14. Vundela, S. R., Kalagatur, N. K., Nagaraj, A., Kadirvelu, K., Chandranayaka, S., Kondapalli, K., Hashem, A., Abd_Allah, E. F., and Poda, S. (2022). Multi-biofunctional properties of phytofabricated selenium nanoparticles from Carica papaya fruit extract: Antioxidant, antimicrobial, antimycotoxin, anticancer, and biocompatibility. *Frontiers in microbiology*, 12, 769891.
15. Nagaraj, A., Ghosh, O. S. N., Ghneim, H. K., AlSheikh, Y. A., Mohammed, K., Poda, S., and Kalagatur, N. K. (2025). Fe_2O_3-type iron oxide nanoparticles from *Aerva lanata* leaf extract exhibit antibiofilm, discriminatory toxicity in cancer cells, and theranostic against oxidative stress in zebrafish. *Chemical Physics Impact*, 100849.
16. Ameh, T., Zarzosa, K., Dickinson, J., Braswell, W. E., and Sayes, C. M. (2023). Nanoparticle surface stabilizing agents influence antibacterial action. *Frontiers in Microbiology*, 14, 1119550.
17. Kakian, F., Mirzaei, E., Moattari, A., Takallu, S., and Bazargani, A. (2024). Determining the cytotoxicity of the Minimum Inhibitory Concentration (MIC) of silver and zinc oxide nanoparticles in ESBL and carbapenemase producing Proteus mirabilis isolated from clinical samples in Shiraz, Southwest Iran. *BMC Research Notes*, 17(1), 40.
18. Niziołek, K., Słota, D., Sadlik, J., Łachut, E., Florkiewicz, W., and Sobczak-Kupiec, A. (2023). Influence of Drying Technique on Physicochemical Properties of Synthetic Hydroxyapatite and Its Potential Use as a Drug Carrier. *Materials*, 16(19), 6431.
19. Bee, S. L., Bustami, Y., Ul-Hamid, A., and

Hamid, Z. A. (2022). Green biosynthesis of hydroxyapatite-silver nanoparticle nanocomposite using aqueous Indian curry leaf (*Murraya koengii*) extract and its biological properties. *Materials Chemistry and Physics*, 277, 125455.

20. Das, T. K., Ganguly, S., Bhawal, P., Mondal, S., and Das, N. C. (2018). A facile green synthesis of silver nanoparticle-decorated hydroxyapatite for efficient catalytic activity towards 4-nitrophenol reduction. *Research on Chemical Intermediates*, 44, 1189-1208.
21. Pai, S., Kini, M. S., Mythili, R., and Selvaraj, R. (2022). Adsorptive removal of AB113 dye using green synthesized hydroxyapatite/magnetite nanocomposite. *Environmental research*, 210, 112951.
22. Imchen, P., Ziekhrü, M., Zhimomi, B. K., and Phucho, T. (2022). Biosynthesis of silver nanoparticles using the extract of *Alpinia galanga* rhizome and *Rhus semialata* fruit and their antibacterial activity. *Inorganic Chemistry Communications*, 142, 109599.
23. Ahmad, E., Athar, A., Nimisha, Zia, Q., Sharma, A. K., Sajid, M., Bharadwaj, M., Ansari, M. A., and Saluja, S. S. (2024). Harnessing nature's potential: *Alpinia galanga* methanolic extract mediated green synthesis of silver nanoparticle, characterization and evaluation of anti-neoplastic activity. *Bioprocess and Biosystems Engineering*, 47(8), 1183-1196.
24. Wei, W., Li, J., Han, X., Yao, Y., Zhao, W., Han, R., Li. R., Zhang, Y., and Zheng, C. (2021). Insights into the adsorption mechanism of tannic acid by a green synthesized nano-hydroxyapatite and its effect on aqueous Cu (II) removal. *Science of The Total Environment*, 778, 146189.
25. Namasivayam, S. K. R., Venkatachalam, G., and Bharani, R. A. (2021). Noteworthy enhancement of wound-healing activity of triphala biomass metabolite-loaded hydroxyapatite nanocomposite. *Applied Nanoscience*, 11, 1511-1530.
26. Vinayagam, R., Kandati, S., Murugesan, G., Goveas, L. C., Baliga, A., Pai, S., Varadavenkatesan, T., Kaviyarasu, K., and Selvaraj, R. (2023). Bioinspiration synthesis of hydroxyapatite nanoparticles using eggshells as a calcium source: Evaluation of Congo red dye adsorption potential. *Journal of Materials Research and Technology*, 22, 169-180.
27. Beigoli, S., Hekmat, A., Farzanegan, F., and Darroudi, M. (2021). Green synthesis of amorphous calcium phosphate nanopowders using *Aloe Vera* plant extract and assessment of their cytotoxicity and antimicrobial activities. *Journal of Sol-Gel Science and Technology*, 98, 508-516.
28. Bhatnagar, S., Kobori, T., Ganesh, D., Ogawa, K., and Aoyagi, H. (2019). Biosynthesis of silver nanoparticles mediated by extracellular pigment from *Talaromyces purpurogenus* and their biomedical applications. *Nanomaterials*, 9(7), 1042.
29. Abdelmigid, H. M., Morsi, M. M., Hussien, N. A., Alyamani, A. A., Alhuthal, N. A., and Albukhaty, S. (2022). Green synthesis of phosphorous-containing hydroxyapatite nanoparticles (nHAP) as a novel nano-fertilizer: preliminary assessment on pomegranate (*Punica granatum* L.). *Nanomaterials*, 12(9), 1527.
30. Sathiyavimal, S., Vasantharaj, S., LewisOscar, F., Pugazhendhi, A., and Subashkumar, R. (2019). Biosynthesis and characterization of hydroxyapatite and its composite (hydroxyapatite-gelatin-chitosan-fibrin-bone ash) for bone tissue engineering applications. *International journal of biological macromolecules*, 129, 844-852.
31. Kumar, R., Shikha, D., Sinha, S. K., Guerra-López, J. R., and Aboudzadeh, N. (2024). Assessment of antioxidant activity, thrombogenicity and MTT assay of bioceramic phosphate as a biomaterial. *Journal of the Australian Ceramic Society*, 1-11.

32. Kalagatur, N. K., Abd_Allah, E. F., Poda, S., Kadirvelu, K., Hashem, A., Mudili, V., and Siddaiah, C. (2021). Quercetin mitigates the deoxynivalenol mycotoxin induced apoptosis in SH-SY5Y cells by modulating the oxidative stress mediators. *Saudi journal of biological sciences*, 28(1), 465-477.
33. Hassanain, M., Abdel-Ghafar, H. M., Hamouda, H. I., El-Hosiny, F. I., and Ewais, E. M. (2024). Enhanced antimicrobial efficacy of hydroxyapatite-based composites for healthcare applications. *Scientific Reports*, 14(1), 26426.
34. Dixit, N.M., Kalagatur, N.K., Poda, S., Kadirvelu, K., Behara, M. and Mangamuri, U.K. (2022). Application of *Syzygium aromaticum*, *Ocimum sanctum*, and *Cananga odorata* essential oils for management of Ochratoxin A content by *Aspergillus ochraceus* and *Penicillium verrucosum*: An in vitro assessment in maize grains. *Indian Journal of Biochemistry and Biophysics*, 59, 172-182.
35. Efenberger-Szmechtyk, M., Nowak, A., Czyżowska, A., Śniadowska, M., Otlewska, A., and Żyżelewicz, D. (2021). Antibacterial mechanisms of Aronia melanocarpa (Michx.), Chaenomeles superba Lindl. and Cornus mas L. leaf extracts. *Food Chemistry*, *350*, 129218.
36. Kalagatur, N. K., Nirmal Ghosh, O. S., Sundararaj, N., and Mudili, V. (2018). Antifungal activity of chitosan nanoparticles encapsulated with *Cymbopogon martinii* essential oil on plant pathogenic fungi *Fusarium graminearum*. *Frontiers in pharmacology*, 9, 610.